Chemical Engineering Science 121 (2015) 300–312

Contents lists available at ScienceDirect

Chemical Engineering Science

journal homepage: www.elsevier.com/locate/ces

Molecular dynamics as a tool to study heterogeneity in zeolites – Effect of Na^+ cations on diffusion of CO_2 and N_2 in Na-ZSM-5

David Newsome [a,b], Marc-Olivier Coppens [c,*]

[a] CFD Research Corporation, 701 McMillian Way, Huntsville, AL 35806, USA
[b] Technical University of Delft, Delft Chem Tech, Julianalaan 136, 2628 BL Delft, The Netherlands
[c] University College London, Department of Chemical Engineering, Torrington Place, London WC1E 7JE, United Kingdom

HIGHLIGHTS

- Diffusion in Na-ZSM-5 zeolite is strongly affected by Al and Na^+ cations.
- MD simulations quantify the effects on diffusion of quadrupolar guest molecules.
- CO_2, with its larger quadrupolar moment, is more strongly affected than N_2.
- A coarse-grained site-lattice representation for the pore network is derived.
- Molecular residence times and probabilities to hop between sites are calculated.

ARTICLE INFO

Article history:
Received 3 June 2014
Received in revised form
8 September 2014
Accepted 13 September 2014
Available online 22 September 2014

Keywords:
Zeolite
Na-ZSM-5
Silicalite-1
Molecular dynamics
Diffusivity
Residence time

ABSTRACT

Zeolites typically contain extra-framework cations to charge-compensate for trivalent Al atom substitutions in the SiO_2 framework. These cations, such as Na^+, directly interact with quadrupolar guest molecules, such as CO_2 and N_2, which move through their micropores, causing energetic heterogeneity. To assess the effects of heterogeneity in Na-ZSM-5 on diffusion of CO_2 and N_2, molecular dynamics (MD) simulations are carried out. In silicalite-1, the pure-silicon form of ZSM-5, the self-diffusivity exhibits a monotonic decrease with molecular loading, while the corrected diffusivity shows a relatively constant value. In contrast, the Na^+ cations cause a maximum or a flat profile over molecular loading for the self- and corrected diffusivities of CO_2 at $T=200$ and 300 K, while the cations only have minimal impact on the diffusivity of N_2. The MD simulations allow us to identify energy basins or sites at which guest molecules spend a relatively long time, and construct a coarse-grained lattice representation for the pore network. Average residence times at these sites are calculated for both species. The trends observed in the residence times correlate to the trends observed in the diffusivity. The residence times for CO_2 at $T=200$ K are long at low loading, but decrease with loading as additional CO_2 molecules compete to stay close to a cation. In contrast, the residence times for N_2 are relatively insensitive to the cations, only mildly increasing near a cation. This difference in behavior can be associated to the quadrupole moments of these molecules.

1. Introduction

This article serves a dual purpose. First, it explores the use of molecular dynamics simulations as a way to probe the heterogeneity of zeolites, especially when Al and charge-balancing cations are present. Tightly confined molecules in the micropores of zeolites mostly reside around stable energy basins or "sites", and diffuse through the pore space by jumping over activation energy barriers between these sites. This leads to a complex dependence on loading for the self- and corrected diffusivities of the molecules, which are hindered by each other and affected by non-uniform interactions with their heterogeneous environment. Calculating the residence times of molecules around various sites, and the barriers between those sites, allows us to parameterize a coarse-grained lattice model that can be used in macroscopic chemical engineering applications. The second purpose of this article is to illustrate this methodology by applying it to a relevant problem: N_2 and CO_2 diffusion in Na-ZSM-5. The (different) quadrupolar moment of these molecules leads to rich diffusion behavior.

CO_2 is present in large quantities in combustion gases from fossil fuel power plants and chemical industries. Because it is a greenhouse gas, energy efficient technology needs to be developed

* Corresponding author.
E-mail address: m.coppens@ucl.ac.uk (M.-O. Coppens).

http://dx.doi.org/10.1016/j.ces.2014.09.024

to capture the CO_2 from flue gases, in which it is typically mixed with N_2 and CH_4 (Liu et al., 2009), to concentrate it for long-term sequestration or reutilization in other chemical processes. Current flue gas separation systems are often based on (amine) solvent absorption and desorption. However, this requires substantial heating to maintain the temperature differences that drive this separation. By comparison, membrane separations utilize differences in adsorption affinity and diffusion rate of molecular species in the material that constitutes the active membrane layer. These differences are controlled by atomic-scale differences in size, shape, and electronic configuration. Major advances have been made in membrane operations and pressure swing adsorption using nanoporous materials as the active layer (Liu et al., 2009).

One class of nanoporous material is zeolites, which are thermally stable and inorganic aluminosilicate crystals with pore widths generally below 1.2 nm, such as DDR and SAPO-34 (~3 Å), ZSM-5 (~5.5–5.7 Å), and FAU (~7 Å). These zeolites have different pore network topologies: constrained cages (DDR), narrow pores joined at intersections (ZSM-5), and large cages joined by narrow windows (FAU). A simplified schematic of the ZSM-5 pore network is featured in Fig. 1a, showing the straight and sinusoidal channels, which meet at intersections. Zeolites consist of a SiO_2 framework, but trivalent Al atoms can replace the tetravalent Si atoms during synthesis. A local charge deficit develops as a result of introducing Al, requiring the presence of an extra-framework cation to maintain a neutral net charge. These cations play an important role, as they exert strong electrostatic interactions on ions, polar and quadrupolar molecules, such as CO_2 and N_2. The strong Coulombic interactions create energetic heterogeneity, as the guest species find deeper energy basins next to the cations. In principle, ion exchange could be used to adjust the type and concentration of cations to tune the energetic heterogeneity, affecting the adsorption and separation performance of zeolites in gas storage and membranes. The extent of Al atoms and cations in the zeolite is designated by the Si to Al atomic ratio (Si/Al). ZSM-5, for example, can contain up to eight Al atoms per unit cell, yielding Si/Al > 11. When Si/Al=∞ no cations are present and the ZSM-5 is designated as silicalite-1. Prior studies have focused on a wide range of cations from Group I and II, such as H^+, Na^+, Rb^+, Li^+, K^+, Cs^+, and Ba^{2+}, and their effects on adsorption and, to a lesser extent, diffusion (Bonelli et al., 2000; Choudhary et al., 1992; Harlick and Tezel, 2002, 2003, 2004; Katoh et al., 1998, 2000; Koriabkina et al., 2002, 2005; Masuda et al., 1998; Newsome et al., 2014; Walton et al., 2006; Wirawan and Creaser, 2006a, 2006b).

Many research groups have performed experimental studies of the adsorption of CO_2, N_2, and CO in activated carbons and zeolites, such as ZSM-5 and FAU, that were impregnated with various cations at T=300–473 K, observing a strong dependence of adsorption capacity to the cation size and strengths of the energetic heterogeneity (Bonelli et al., 2000; Calleja et al., 1998; Dunne et al., 1996a, 1996b; Harlick and Tezel, 2002, 2003, 2004; Katoh et al., 1998, 2000; Koriabkina et al., 2002, 2005; Masuda et al., 1998; Siriwardane et al., 2001; Walton et al., 2006; Wirawan and Creaser, 2006a, 2006b). CO_2 molecules have a stronger quadrupolar moment than N_2 or CO, so that CO_2 binds more strongly to the cations. A lower Si/Al ratio systematically increases the amount of adsorbed CO_2 at a given pressure, whether in a pure component form or in a mixture. Larger cations, like Na^+ and Ba^{2+}, interact more strongly with CO_2 than H^+, with CO_2 in H-ZSM-5 showing an adsorption behavior similar to that in silicalite-1 (Bonelli et al., 2000; Calleja et al., 1998; Dunne et al., 1996a, 1996b; Katoh et al., 1998, 2000; Wirawan and Creaser, 2006a, 2006b).

Experimental methods also exist to quantitatively assess transport properties of molecular diffusion in porous materials. The Constant Volume Method, (Masuda et al., 1998) Positron Emission Profiling, (Koriabkina et al., 2002, 2005) Pulsed Field Gradient-Nuclear Magnetic Resonance (PFG-NMR), (Hedin et al., 2008; Kärger et al., 1993, 2012; Kärger and Pfeifer, 1991) and Quasi-Elastic Neutron Scattering (QENS) (Jobic et al., 2004; Jobic and Theodorou, 2007) have been applied to study experimentally the diffusion of gas molecules in zeolites, such as CO_2, N_2, CH_4, C_2H_6, benzene, p-xylene, and hexane in ZSM-5. These studies show how diffusivities depend on the shape and dimensions of the pore network and the guest molecules. Koriabkina et al. and Masuda et al. found that H^+ cations in ZSM-5 cause a dramatic decrease in the diffusivity of the large molecules benzene, toluene,

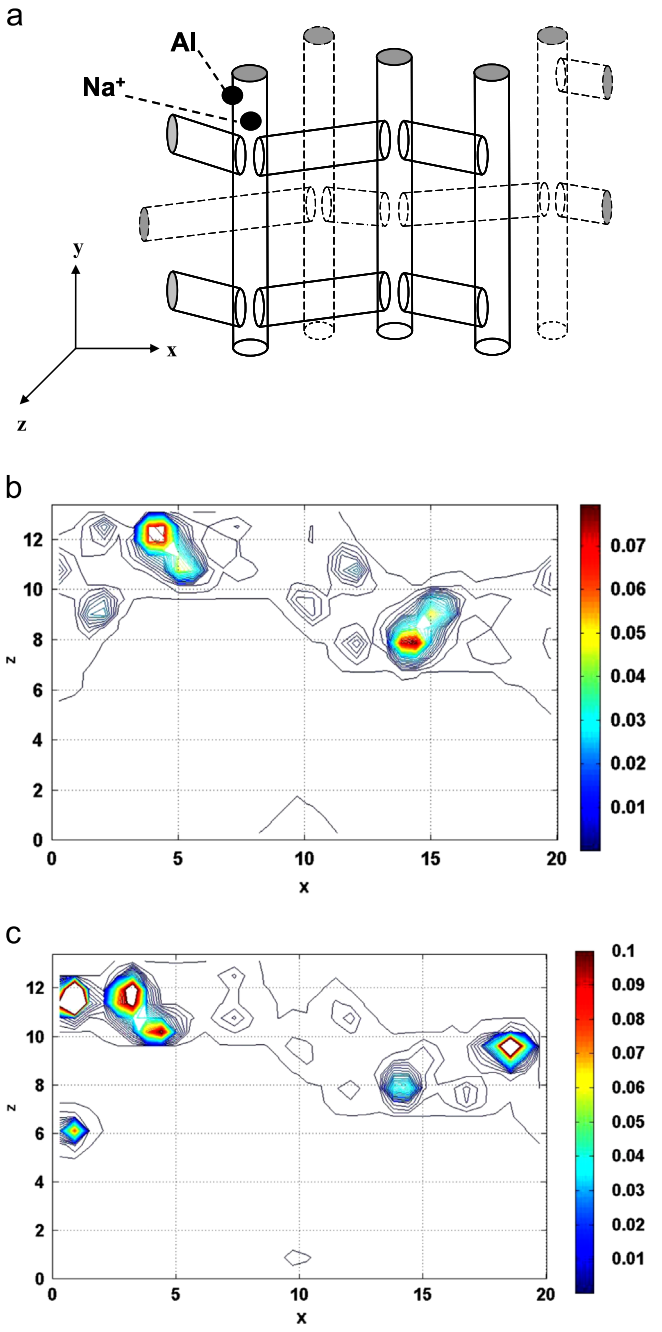

Fig. 1. (a) Simplified schematic of the ZSM-5 pore network, showing the channel structure for the orthorhombic MFI framework. Coordinates are in Å. Lattice parameters: a=20.1 Å, b=19.9 Å, c=13.4 Å. Isodensity plots for 4 CO_2/Unit Cell and 200 K. (b) The cross-sections at constant y-plane (y=4.88 Å) for higher density levels (in $Å^{-3}$) in silicalite-1, showing the stable basins of a sinusoidal channel, and (c) the isodensity plot at a single constant y-plane for Na-ZSM-5 with 1 Al and Na^+/Unit Cell. The local density levels of the stable basins surrounding the Na^+ cation are substantially increased.

p-xylene, hexane, and 2-methylpentane, in the range of T= 393–723 K. The cations impact diffusion more severely at lower loading and lower temperature.

As a complement to experimental measurement of diffusivities, atomically detailed molecular dynamics (MD) simulations provide theoretical insight and quantitative predictions of molecular diffusion in zeolites. Simulation results have been compared to experimental studies of PFG-NMR and QENS, showing encouraging agreement (Chong et al., 2005; Goj et al., 2002; Jobic et al., 2004; Kärger et al., 1993; Papadopoulos et al., 2004). Similarly, grand canonical Monte Carlo (GCMC) has provided many examples of quantitative predictions of light gas adsorption in zeolites and compared well to experimental adsorption measurements (Newsome et al., 2014). MD and GCMC have been applied to study the behavior of light gases in many zeolites. For example, Sholl, Kohen, and coworkers studied CH_4, CF_4, and CO_2, in a variety of pure-silica zeolites (silicalite-1, ITQ-3, ITQ-7, and ZSM-12), demonstrating various types of behavior as a function of loading, pore topology, and molecular size (Goj et al., 2002; Selassie et al., 2008; Skoulidas et al., 2003; Skoulidas and Sholl, 2003, 2002). Makrodimitris, Papadopoulos, Jobic, and Theodorou ran MD and GCMC simulations of CO_2 and N_2 in silicalite-1 (Makrodimitris et al., 2001; Papadopoulos et al., 2004). Their simulations demonstrated the preferential adsorption of CO_2 over N_2 due to strong electrostatic attractions with the zeolite framework, and also showed that the diffusivity of CO_2 is substantially lower than that of N_2. At this time, MD is usually limited to diffusivities $> 10^{-11}$ m^2/s; slower transport can be analyzed with transition state theory (TST) or transition path sampling (TPS) methods. Jee and Sholl (2009) performed simulations of CO_2 and CH_4 in DDR zeolites, using MD combined with TST to analyze the faster diffusion of CO_2 in mixtures with slowly diffusing CH_4. Vlugt et al. (2000) used MD combined with TPS to analyze the hindered motion of isobutane in silicalite-1. Hirotani et al. (1997) used GCMC to analyze the role of Na^+ cations in ZSM-5, observing an enhanced adsorption of CO_2. Beerdsen et al. (2002, 2003) carried out GCMC simulations to study the role of a variety of cations on the adsorption of CH_4, C_2H_6, C_3H_8, and C_4H_{10} isomers in ZSM-5 and MOR, observing strong correlations with cation size and Si/Al. The smaller cations Na^+ and Li^+ led to stronger adsorption relative to the larger cations K^+ and Cs^+, where pore exclusion was a limiting factor. Jia and Murad (2004, 2005) performed MD simulations of CO_2 and N_2 mixtures permeating through faujasite with Na^+, silicalite-1, and chabazite. Demontis et al. (1989, 2008) have demonstrated how MD simulations provide insight into dynamical behavior with cations present in the zeolite.

As a result of strong confinement, diffusion in zeolites is often activated: guest molecules “hop” through the pore network from one adsorption site to another. These sites correspond to free energy wells or stable basins, and guest molecules have to cross activation energy barriers to move from one well to the next. Hence, another key parameter to describe molecular diffusion in zeolites is the residence time, which is the average time period that a molecule spends in a given stable basin. The residence time can also be viewed as the inverse of the low-loading hopping frequency. Experimental methods are not yet capable of directly resolving the residence times. However, MD simulations are able to calculate the average time molecules spend in a stable basin. These show that molecules spend more time near the cations, defined as strong basins, while spending less time in the energetically more shallow, weak basins, as they can hop out of these basins more frequently. For many pure-silica systems, hopping is sufficiently frequent that the diffusivities can be directly calculated from the MD trajectory data. However, MD as a stand-alone method is not practical for extended, macroscopic systems. In those cases, a multi-scale approach should be used, in which residence times are inserted into a coarse-grained lattice model. Lattice model based estimates, including dynamic Monte Carlo (DMC) simulations and mean field theory (MFT), use a bond and node lattice description of the zeolite network. This coarse-grained approach allows calculations on length and time scales not easily accessible with stand-alone MD (Auerbach, 2000; Dellago et al., 2001; Frenkel and Smit, 2002; Keil et al., 2000; Saravanan et al., 1999; Saravanan and Auerbach, 1997a, 1997b; Smit and Maesen, 2008; Theodorou et al., 1996; Vlugt et al., 2000). Other methods include MD runs at higher temperature, so as to provide enough momentum to achieve activation (Ramanan et al., 2004; Schuring et al., 2007), or Monte Carlo techniques (Voter, 1985). In our study, residence times are determined from MD simulations to explain trends in diffusivities.

Diffusivities calculated from MD simulations are presented for silicalite-1 (Si/Al=∞), and ZSM-5 with 1 or 2 Na^+ cations per unit cell (Si/Al=95 and Si/Al=47). For Si/Al=47, the diffusivities are $> 10^{-11}$ m^2/s down to 300 K, so that stand-alone MD can be used. Residence times for CO_2 and N_2 could be determined with stand-alone MD for silicalite-1 and Na-ZSM-5 with Si/Al=95, where diffusivities are $> 10^{-11}$ m^2/s, even at 200 K.

The remainder of this paper is organized as follows. In Section 2 the MD method and the energy parameters used to gather trajectory data are briefly described. Diffusivity and residence time results are presented and discussed in Section 3. Conclusions are summarized in Section 4.

2. Methodology

2.1. Molecular dynamics (MD) simulations

MD simulations consist of an iterative solution of Newton's equation of motions, providing the positions and velocities of atoms in a many-body system over time. The output is a collection of snapshots in time of the trajectories of the atoms, which can be used in subsequent analysis. Using these data sets, physical properties such as diffusivities and residence times can be calculated.

In this work the DL_POLY package was used. This is an open-source MD program from Daresbury Laboratory (2003). The simulations were implemented with the velocity-Verlet integration scheme in a canonical (NVT) ensemble, with the Nosé–Hoover thermostat applied for temperature control. The trajectories were typically run for 200 ps until equilibration, and 13–28 ns for further analysis, using a time step of 4 fs. Trajectory snapshots were collected at 1 ps intervals for later analysis. For many of the simulation state points, 2–20 simulations starting from different initial conditions were executed to allow proper statistical sampling.

The zeolite lattice atom positions were taken from the experimental work of van Koningsveld et al. (1987), to construct an entire ZSM-5 unit cell (Beerdsen et al., 2003). A simulation box of 27 ZSM-5 unit cells was used, with three unit cells in each orthogonal direction. The structure was assumed to be orthorhombic, and belonging to the *Pnma* space group for all temperatures, though it is possible that the crystalline structure (and space group) vary with temperature (Makrodimitris et al., 2001; Skoulidas and Sholl, 2002; van Koningsveld et al., 1987). This box size is large enough to maintain a sufficiently high population of molecules and to fulfill the minimum image convention, so that the molecules do not see their periodic ghost image when periodic boundary conditions are applied (Frenkel and Smit, 2002). The interaction parameters were collected from prior literature sources, as summarized in Tables 1 and 2. Both long-range Coulombic and short-range dispersion forces were used to describe the guest–guest atom and guest–zeolite atom interactions.

Table 1
List of potential energy parameters. For the guest atom sites (C, O_G, N), the Lorentz-Berthelot mixing rules were applied for the cross-atomic interactions, so that only the self-interaction terms are included.

Atom pairs	ε [kJ/mole]	σ [Å]	Reference
C–C	0.2245	2.80	Potoff and Siepmann (2001)
O_G–O_G	0.6568	3.05	Potoff and Siepmann (2001)
N–N	0.30264	3.318	Makrodimitris et al. (2001)
Na–Na	2.5325	2.33	Beerdsen et al. (2002)
Na–C	0.1746	2.7217	Hirotani et al. (1997)
Na–O_G	0.2946	2.833	Hirotani et al. (1997)
Na–N	0.87547	2.824	Lorentz-Berthelot average
Si–Guest	0	0	Makrodimitris et al. (2001)
Si–Na	2.5325	2.33	Beerdsen et al. (2002)
O_Z–Guest	0.745	2.806	Makrodimitris et al. (2001)
O_Z–Na	2.5325	2.33	Beerdsen et al. (2002)
Al–C	0.1965	1.9021	Hirotani et al. (1997)
Al–O_G	0.3316	2.0134	Hirotani et al. (1997)
Al–N	0.3316	2.0134	Assumed same as Al–O_G
Al–Na	2.5325	2.33	Beerdsen et al. (2002)

Table 2
List of the Coulombic charges for each atom site, in terms of the elementary charge. The * refers to cases with Al framework substitution, which requires changes in the partial charges. The first charge refers to the case of silicalite-1, while the second value refers to ZSM-5 with Al and Na^+.

Atom Site	q [e]	Reference
C	+0.7	Potoff and Siepmann (2001)
O_G	−0.35	Potoff and Siepmann (2001)
Z_M	+0.80968	Makrodimitris et al. (2001)
N	−0.40484	Makrodimitris et al. (2001)
Na	+1	Beerdsen et al. (2002)
Si*	+2/+2.05	Makrodimitris et al. (2001)/Beerdsen et al. (2002)
O_Z*	−1/−1.025	Makrodimitris et al. (2001)/Beerdsen et al. (2002)
Al	+1.75	Beerdsen et al. (2002)
O_{Al}	−1.2	Beerdsen et al. (2002)

The Ewald summation algorithm was used to model the guest–guest Coulombic forces, with a real-space cut-off radius of 20 Å. Due to the large number of zeolite atoms present, the pretabulation algorithm for long-range forces described in Makrodimitris et al. (2001) and Skoulidas and Sholl (2002) was employed. Ten surrounding layers of the ZSM-5 unit cell are created around a single central unit cell. Then, the potential energy, force, and higher order derivatives of the force between a ghost position of charge +1e in the unit cell and each zeolite atom in this larger crystal structure are calculated using Coulomb's law. A ghost position is systematically placed on grid points with a spacing of ~0.2 Å, with the results pretabulated in an external file for later use. The interpolation scheme described by Skoulidas and Sholl (2002) is used to get the final force on a specific atom during the MD simulation . The final force result is multiplied by the charge of the specific atom, as this is a common factor that can be included in the final step. The pretabulation was made over the entire unit cell, since cations are now present, which destroys the symmetry of the system.

The short-range forces were modeled using the Lennard-Jones 6–12 potential form for all interaction pairs. The zeolite contribution for the short-range forces was also pretabulated and interpolated in the same manner as the long-range forces, but this step took mere minutes and was performed at the start of each simulation. This is because the short-range forces are well approximated using a cut-off radius of 13 Å, thus only require two unit cells in each direction. In the actual crystal structure, the framework vibrates. However, for smaller molecules, such as N_2 and CO_2, these vibrations can be safely ignored (Makrodimitris et al., 2001; Skoulidas and Sholl, 2002).

CO_2 molecules are modeled as a linear triatomic molecule, with two covalent bonds of length 1.16 Å between the C and O atoms. N_2 is also treated as a linear triatomic molecule with a single covalent bond of 1.10 Å between the N atoms. A central fictional site of zero-mass with a positive partial charge is inserted between the N atoms. This third site is included to maintain a proper charge distribution when modeling the quadrupole moment and is therefore defined without any dispersion interactions, as implemented in Makrodimitris et al. (2001) and Goj et al. (2002). The quadrupole moment of N_2 is $Q = -4.67 \times 10^{-40}$ C m^2, while that for CO_2 is $Q = -13.67 \times 10^{-40}$ C m^2. Makrodimitris et al. (2001) tested this feature for N_2, determining that the presence of charges as a three-site distribution gave better agreement with experimental adsorption isotherms, compared to a two-site dumb-bell model without any charges.

Initial configurations were made with a separate pre-processing algorithm. The algorithm randomly inserted the central atom of the three-site model and then grew the second and third atoms along opposite ends of a random vector, which was scaled to the length of the covalent bonds. A trial initial position of a molecule was accepted if each atom was at least 2.5 Å from the zeolite atoms and other prior inserted guest atoms. This length of 2.5 Å was empirical; shorter lengths caused the MD runs to stop in error, as the initial overlap with other atoms would be too great, while longer lengths prevented the algorithm from inserting molecules, especially at higher loadings.

The Na^+ cations were inserted using the same overlap entry criteria as for the guest molecules but with a randomly oriented distance of 2.8 Å from a pre-chosen Al atom at the intersections. This length is also empirical, but was chosen thus as it is a typical dispersion interaction length. During the MD equilibration the Na^+ cations relaxed into positions nearby the Al atoms. They vibrated but never diffused away during the course of the simulations due to the strong Coulombic attraction with the lattice charge deficit.

2.2. Diffusivities

The self-diffusivity, D_S, measures the tracer motion of individual molecules and is defined by the well-known Einstein relationship

$$D_S = \lim_{t\to\infty} \frac{1}{6t} \left\langle \frac{1}{N} \sum_{i=1}^{N} \left| \vec{r}_i(t) - \vec{r}_i(0) \right|^2 \right\rangle. \quad (1)$$

Similarly, the corrected-diffusivity D_0, which measures the collective motion, is defined as:

$$D_0 = \lim_{t\to\infty} \frac{1}{6t} \left\langle \left| \frac{1}{N} \sum_{i=1}^{N} \left[\vec{r}_i(t) - \vec{r}_i(0) \right] \right|^2 \right\rangle. \quad (2)$$

At low loading, $D = D_0 = D_S$. However, at higher loadings, correlations between the trajectories of individual molecules mean that $D_0 \neq D_S$. Theodorou et al. (1996) and Skoulidas and Sholl (2002) discuss these diffusion properties in more detail.

Self- and corrected diffusivities can be calculated from the MD trajectory data. The procedure described in Frenkel and Smit was used to construct a linear plot of the mean squared displacement (MSD) over time, using post-process analysis algorithms to calculate D_S and D_0 (Frenkel and Smit, 2002). In Eq. (1) the tracer motion of each molecule makes a unique contribution to the calculation of the MSD. In contrast, the collective MSD in Eq. (2) is based on the motion of the center of mass of a swarm of molecules, and not the many more, individual contributions from each molecule separately. As a result, the number of samples is substantially smaller compared to the MSD for self-diffusion, thus is more prone to noise, especially at longer times. Since the

statistics are inherently poor, 20 simulations were implemented at any given state point, but initialized for unique initial configurations. The statistics of the self-diffusivities were excellent; the MSD plots showed nice linear trends after 50 ps to a few ns. The collective MSD plot showed more pronounced curvature at longer times, due to the expected sampling limits, even after combining data from the 20 simulations of each state point. Therefore, as a practical necessity, the linear fit was made over a shorter time frame of a few ns, where the MSD showed a clear linear trend due to the inclusion of more data samples. For the case studies for Si/Al=95 and 47 at T=200 and 300 K, the molecules spend much of their time nearby the cations. The slow motion in these case studies leads to a longer transition time of a few ns. Therefore, the self-diffusivities were fitted only after a few ns elapsed, say 2–4 ns, and based on a MSD averaged over a period of 15 ns or more. A 95% confidence interval at each snapshot in time of a MSD plot was determined, and then used to rerun the linear fit to check the sensitivity. The error bars were only a few percent of the values of the diffusivities in all cases, since many displacement samples were included in the averaging.

2.3. Stable basin definitions

Stable basins or sites correspond to sub-volumes that have a relatively higher occupational probability or density, as observed from the MD trajectories. Molecules spend a high proportion of their time in these basins. To define them, a unit cell is first discretized into volume elements, or voxels, of edge size ~0.6 Å. The local density of each voxel is determined, which is proportional to the average Boltzmann weight for the voxel. From each snapshot in time the actual location of the center of mass of a molecule is backtracked to its position in a single unit cell; each of the three coordinates is divided by the voxel length to determine the voxel indices. The average density for any voxel is defined as the average residence tally per unit voxel volume taken over many snapshots.

2.4. Placement of the Na^+ cations

For ZSM-5 the cations can be inserted into either channels or intersections. Beerdsen et al. (2003) placed the cations into both intersections and channels, using only certain tetrahedral sites for substitutions. Other computational studies have used DFT to determine the energetically preferable location of the framework substitutions in ZSM-5. Placement of Na^+ cations in channel sites creates more pore blockage, as molecules would have less room to bypass the cation. Aoki et al. (2000) performed permeance measurements in ZSM-5 with framework substitutions. Based on the separation of butane isomer mixtures, they speculated that, at least for their samples, the cations were likely positioned in the more spacious intersection regions. Prior lattice studies by Coppens et al. (Coppens et al., 1999; Coppens and Iyengar, 2005; Iyengar and Coppens, 2004) assumed the strong sites to be in the intersections as well. Following this work, the Na^+ cations and Al framework substitutions were placed in the intersection region of the ZSM-5 unit cell.

Simulations were carried out for 0, 1 and 2 Al/Unit Cell (Si/Al=∞, 95, and 47). The Al framework substitutions were made at the Si atom positions of $\vec{r}$ ={3.73, 1.17, 8.99} Å and $\vec{r}$ ={6.27, 11.13, 2.30} Å (where positions are set with the origin at the lower corner of the unit cell). Fig. 1b and c presents isodensity contour plots (units of $Å^{-3}$) that compare the pattern of the potential energy landscape of ZSM-5 in the forms of Si/Al=∞ and 95 for a cross-section of a sinusoidal channel. The isocontours plot was constructed using the 'contourslice' function in Matlab. The contour lines are drawn to represent constant density values within the voxels at a given fixed plane. In Fig. 1b (for silicalite-1) no cation is present, thus the two shown stable basins are energetically similar. Interestingly, it is the channel basins that are energetically stable, corresponding to higher density levels, while the intersections have lower density levels. In contrast, for Na-ZSM-5 with Si/Al=95, as presented in Fig. 1c, the local density contours are at higher levels around the Na^+ cation. A clear void space is also seen around the cation due to local volume exclusion. Additional cross-sections are included in Supplementary material.

3. Results and discussion

3.1. Diffusion of CO_2

The self- and corrected diffusivities of pure CO_2 are presented in Fig. 2a–c for (a) T=200 K, (b) 300 K, and (c) 400 K, for Si/Al=∞, 95, and 47, over a typical loading range of 1–14 CO_2/Unit Cell. This range of temperature corresponds to the standard range found in experimental studies of adsorption and permeation for light gases, with most studies around 300 K (Bernal et al., 2004; Bowen et al., 2002; Dunne et al., 1996a, 1996b; Hasegawa et al., 2002; Himeno et al., 2007; Zhu et al., 2006).

For silicalite-1, in the low-loading regime, $D=D_0=D_S=9\times10^{-10}$ m^2/s at 200 K, $D=3.5\times10^{-9}$ m^2/s at 300 K, and $D=7\times10^{-9}$ m^2/s at 400 K. The self-diffusivities for silicalite-1 for all three temperatures monotonically decrease with loading. The CO_2 molecules uniformly distribute along the basins due to energetic homogeneity; crowding leads to an approximately linear drop in self-diffusivity with increased loading (Coppens et al., 1999). The corrected diffusivities, on the other hand, are relatively insensitive to loading over the range of 0–8 CO_2/Unit Cell, a trend previously noted by Skoulidas and Sholl (2002). A favorable comparison of these MD results for both CO_2 and N_2 in silicalite-1 with prior PFG-NMR and QENS experimental measurements is included in Supplementary material, indicating the reliability of this MD force field model and software utilized in this study. Also other groups have compared MD results to these experimental data, indicating good agreement (Jobic and Theodorou, 2007; Makrodimitris et al., 2001; Selassie et al., 2008).

The diffusivities for Na-ZSM-5 with Si/Al=95 show a dramatically different trend for 200 K and 300 K, as presented in Fig. 2a and b. For 200 K, at very low loading (1 molecule per unit cell), the diffusivity is about 4×10^{-11} m^2/s, which is still above the calculation threshold of stand-alone MD. Both the self- and the collective diffusivities increase to a maximum of $2–3\times10^{-10}$ m^2/s for 8–12 CO_2/Unit Cell. For 300 K, the diffusivity for 1 molecule per unit cell is 7×10^{-10} m^2/s, increasing to $9–15\times10^{-10}$ m^2/s for 5–12 CO_2/Unit Cell.

Thus, for Si/Al=95, in the low loading range, the self-diffusivities initially increase with loading. The CO_2 molecules preferentially reside near the cations due to the stronger attraction. Even if they hop into a nearby weaker basin, they still feel the long-range attraction of the Na^+ cation and are prone to return or perhaps hop to another cation, unimpeded by other molecules. At higher loading, the CO_2 molecules compete to interact with the cations. The CO_2 molecules closest to a cation shield this cation from other CO_2 molecules, reducing the strength of the electrostatic interactions, causing faster diffusion and longer residence in the weaker basins. The guest–guest steric hindrance plays a greater role at higher loading, so that the self-diffusivity displays the same monotonic decrease as observed in silicalite-1. The maximum in the diffusivity at 300 K is clearly less pronounced, as the higher temperature reduces the attractive influence of the cation.

The corrected diffusivities of pure CO_2 in Na-ZSM-5 with Si/Al=95 at 200 K (Fig. 2a) and at 300 K (Fig. 2b) show the same initial

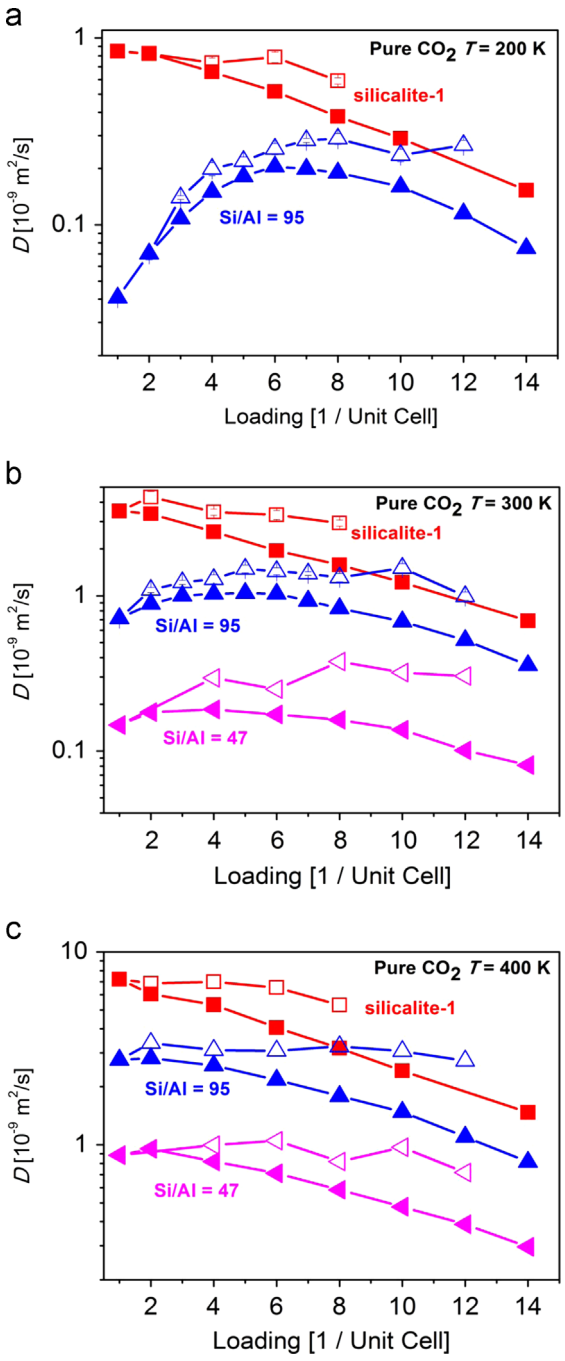

Fig. 2. Self- and corrected-diffusivities of CO_2 at (a) 200, (b) 300, and (c) 400 K over the range of 1–14 CO_2/Unit Cell. Red squares are for pure CO_2 at Si/Al=∞ (silicalite-1). Blue triangles are for Si/Al=95. Magenta triangles are for Si/Al=47. The self-diffusivities are shown as solid symbols, while the hollow symbols are the corrected diffusivities. (For interpretation of the references to color in this figure legend, the reader is referred to the web version of this article.)

increase at low loading as the self-diffusivities. Recall that, by definition, at low loading the self-diffusivity equals the corrected diffusivity. At higher loading the correlation effects manifest themselves, and the corrected diffusivities become consistently larger than the self-diffusivities, showing a weak dependence with loading instead of the monotonic decrease seen for silicalite-1.

The self- and corrected diffusivities of CO_2 for Si/Al=95 at 400 K are presented in Fig. 2c. They no longer show an increase in the low-loading range, for the higher temperature substantially reduces the interaction strength induced by the cations. At low loading, $D=3\times10^{-9}$ m^2/s. The self-diffusivity decreases in a monotonic manner to 9×10^{-10} m^2/s for 14 CO_2/Unit Cell, while the corrected diffusivity remains essentially independent of loading.

For the case of Si/Al=47 the self- and corrected diffusivities are presented for 300 K and 400 K in Fig. 2b and c, respectively. They were not determined for 200 K, as diffusion is too slow to lead to reasonably accurate estimates from stand-alone MD. Even for Si/Al=95 at 200 K, stand-alone MD is near the threshold of 10^{-11} m^2/s. At 300 K and low loading, $D=1.5\times10^{-10}$ m^2/s. The self-diffusivity slightly increases to a maximum of 1.8×10^{-10} m^2/s around 3–4 CO_2/Unit Cell, then decreases in a similar, monotonic manner to $D=8\times10^{-11}$ m^2/s for 14 CO_2/Unit Cell. The corrected diffusivities remain consistently larger, increasing to a relatively constant value of $D=3\times10^{-10}$ m^2/s in the range of 4–12 CO_2/Unit Cell. At this temperature diffusion is sufficiently fast that stand-alone MD can be used, even though now there are two cations/Unit Cell. Due to the larger number of cations per Unit Cell for Si/Al=47, the diffusivities are ~1/4 of the values for Si/Al=95.

The diffusivity for Si/Al=47 and 400 K at low loading is $D=9\times10^{-10}$ m^2/s. The self-diffusivity decreases to 3×10^{-10} m^2/s, while the corrected diffusivity shows a much weaker dependence on loading over the range 4–12 CO_2/Unit Cell. These trends are similar to those observed in silicalite-1, as the cations have a reduced impact at this higher temperature.

3.2. Diffusion of N_2

To assess the effect of its lower quadrupole moment, analogous simulations were performed for N_2 at 200 and 300 K. Though N_2 has a larger kinetic radius than CO_2, its quadrupole moment is about 1/3 of the value for CO_2, so that N_2 molecules will diffuse faster compared to CO_2, due to weaker Coulombic interactions with the cations. The diffusivities of N_2 for Si/Al=∞, 95, and 47 at 200 K and 300 K are featured in Fig. 3a and b. At low-loading and 200 K $D=8\times10^{-9}$ m^2/s for silicalite-1, $D=5\times10^{-9}$ m^2/s for Si/Al=95, and $D=3\times10^{-9}$ m^2/s for Si/Al=47. For 300 K the low-loading diffusivities are $D=1.7\times10^{-8}$ m^2/s for silicalite-1, $D=1.1\times10^{-8}$ m^2/s for Si/Al=95, and $D=7.0\times10^{-9}$ m^2/s for Si/Al=47. Results in silicalite-1 are also compared to published experimental data in Supplementary material, showing reasonable agreement for the N_2 model in this MD algorithm. The diffusivities for N_2 at very low loading in silicalite-1 could not be determined. The N_2 molecules were observed to get caught in a local symmetry site of the zeolite lattice, where they rapidly rotated. This unnatural movement caused the thermostat to respond by removing momentum from all other molecules, leading to an artificial freezing problem. This problem did not occur at higher loading, since molecular collisions pushed molecules away from the symmetry site and prevented this unnatural rotation. Hence the low loading diffusivity at 1 N_2/Unit Cell in Fig. 3a and b is a linear extrapolation from the higher loading values. This extrapolation was carried out to maintain a complete set of diffusivities for N_2 in silicalite-1 over all loadings.

The self-diffusivity of N_2 in Na-ZSM-5 with Si/Al=95 and 47 shows the same monotonic decrease as in silicalite-1, in contrast to CO_2, which shows an initial increase with loading for both 200 and 300 K, before decreasing at higher loading. The self-diffusivity of N_2 is less sensitive to the Si/Al ratio than the self-diffusivity of CO_2, and values are typically an order of magnitude larger, indicating the strong impact of the quadrupole moment. Though the self-diffusivity of N_2 shows the same qualitative pattern for all Si/Al ratios, the values systematically decrease with lower Si/Al, due to weaker electrostatic interactions and pore blockage. Like for CO_2, but even more pronounced, the corrected diffusivity of N_2 is relatively insensitive to loading in all situations.

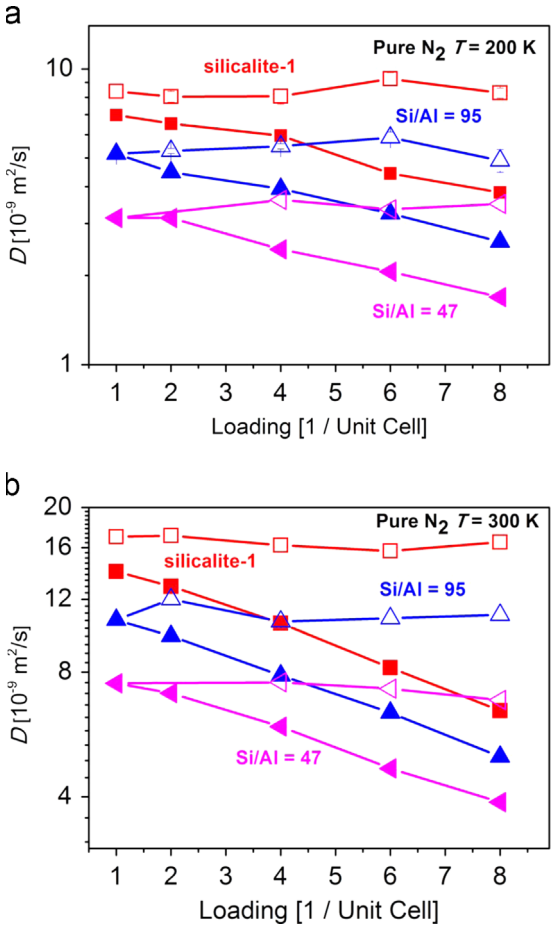

Fig. 3. Self- and corrected-diffusivities for N_2 at (a) 200 and (b) 300 K at Si/Al=∞, 95, and 47. The same symbol scheme from Fig. 2 applies.

3.3. Activation energy barriers

The activation energy barriers, E_a, are presented in Fig. 4 for both CO_2 and N_2 for Si/Al=∞, 95, and 47. An Arrhenius fit was made for the self-diffusivity based on the calculations at 200, 300 and 400 K. While this range is narrow, the results are informative. The activation barrier of N_2 for silicalite-1 is E_a=3 kJ/mole and, for CO_2, E_a=6.8 kJ/mole, irrespective of loading, due to the energetic homogeneity of the potential energy landscape in silicalite-1. For Na-ZSM-5 with Si/Al=95, E_a=3.5 kJ/mole for N_2, independent of loading. The small increase in activation barrier for N_2 when cations are present is due to the slightly stronger interaction between N_2 and the cations. In strong contrast, and analogous to the diffusivities, a different trend is observed for the CO_2 activation energy barrier in Na-ZSM-5 with Si/Al=95. At 2 CO_2/Unit Cell, where the Na^+ cation is more exposed, E_a=12.5 kJ/mole, then decreases as a function of loading to 7 kJ/mole at 8 CO_2/Unit Cell. For Si/Al=47, the activation energy barrier of N_2 is E_a=4 kJ/mole and remains constant as a function of loading. In contrast, the activation energy barrier of CO_2 depends on loading, with E_a=16 kJ/mole at 2 CO_2/Unit Cell, decreasing to 14 kJ/mole over the range from 2 to 8 CO_2/Unit Cell. The presence of the second cation per unit cell increases the overall activation energy barrier for long-range diffusion. In the presence of more cations, the CO_2 molecules become less effective in counter-balancing the electrostatic charge of the cations.

3.4. Concept of residence times

The residence time for a site or a basin is defined as the average time that a molecule spends in a stable basin before hopping to a neighboring stable basin. Many prior studies have applied MD to assess rate constants for transport in nanoporous materials (Auerbach, 2000; Dellago et al., 2001; Frenkel and Smit, 2002; Jee and Sholl, 2009; Jousse and Auerbach, 1997; June et al., 1991; Saravanan et al., 1999; Saravanan and Auerbach, 1997a, 1997b; Vlugt et al., 2000; Voter, 1985). In this work, residence times are determined by accumulating values of a binary characteristic function over the course of the trajectory time length for all molecules. The binary characteristic function for a stable basin α is defined as

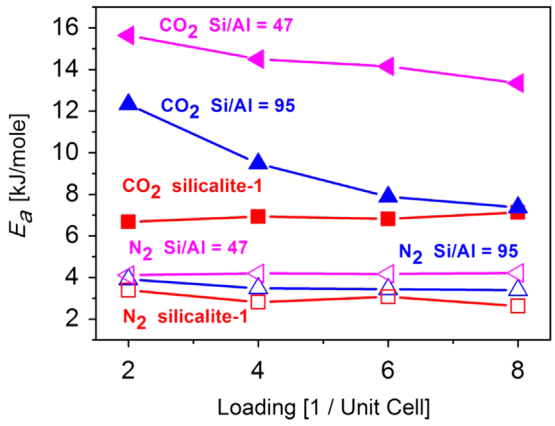

Fig. 4. The activation energy barriers E_a for CO_2 and N_2 over a range of loading. The E_a results were taken from the Arrhenius analysis of the self-diffusivities.

$$h_\alpha = \begin{cases} 0 & \text{if the molecule is not in the stable basin } \alpha \\ 1 & \text{if the molecule is in the stable basin } \alpha \end{cases} \quad (3)$$

so that, at any given time step, h_α is only 1 for the basin associated with the location of the molecule, while, for all other basins, h_α=0. Using this simple quantity, the average residence time is defined as

$$\tau_\alpha = \frac{\sum_{m=1}^{N_m}\sum_{t=1}^{N_t} h_\alpha}{\sum_{m=1}^{N_m} N_{events}} \tau_{Samp} \quad (4)$$

The numerator is a double summation of h_α, first over the set of time steps (N_t) along the entire course of the simulation, then as a second summation amongst the population of molecules (N_m). Multiple simulations were combined to improve the statistical basis. Incomplete residence events at the beginning of the simulations are excluded, such that only those residence periods where a distinct entry and exit event occur are included in the sampling. The denominator is the summation, over all molecules, of the number of residence events for each molecule. An entry event is defined to start at the first time snapshot when all three sites of a CO_2 or N_2 molecule are found to reside in the volume of the stable basin, so that h_α=1. The exit event for this molecule occurs when h_α=1 for a different stable basin. The residence event for the current basin is then considered complete and N_{events} is incremented by 1 for the current basin. In the final step the intermediate calculations are scaled by the sampling period, τ_{samp}=1 ps, to allow for proper time units.

The stable basins are defined such that their volumes are large enough to accommodate the molecules while they are also sufficiently separated by a distance more than the size of a CO_2 molecule. An isosurface plot of the ZSM-5 pore network in Fig. 5a shows the z-oriented projection of the location of CO_2 molecules in silicalite-1 at 200 K. The isosurface plots were constructed using the 'isosurface' function in Matlab. The isosurface was defined to

border the outer layer of the group of voxels with a local density above the threshold value, corresponding to each energetically preferred sub-volume. The threshold density level is set high enough (0.01 $Å^{-3}$) to demonstrate that CO_2 preferentially resides in the channels of silicalite-1, but also resides along the walls of the intersections nearby the channels.

In this perspective the stable basins are distinct and separate. These types of plots were manually analyzed to determine the appropriate sub-volumes that define the channel basins and provided to the residence time algorithm. Interestingly, this shows that the primary basins are the channels, not the intersections. The intersections could also be interpreted as secondary basins; residence time calculations indicate that these regions were not individually activated for CO_2, even at the low temperature of 200 K. Hence, at least for this case, the intersections could be considered as an immediate spatial extension of the channel basins and serve as a separation zone between the channels. Though the molecules can visit the intersections with ease (viz. Fig. 1a), the actual activation occurs in the channels. Fig. 5b is a coarse-grained representation of the ZSM-5 pore network. In this representation the stable basins are treated as nodes, while the spaces at the intersections are collapsed into bonds, corresponding to effective hopping pathways. The eight channel sites per unit cell are labeled as Str1-4 and Sin1-4 for the four straight channels and the four sinusoidal channels, respectively.

3.5. Residence times for CO_2 and N_2 in silicalite-1

Fig. 6 shows the residence times in the sinusoidal and straight channel sites of (a) CO_2 and (b) N_2 for silicalite-1 at 200, 300, and 400 K. These were calculated from the same MD simulations used to calculate the diffusivities. For CO_2 at low loading, the residence times are τ=98–125 ps at 200 K, τ=30–33 ps at 300 K, and τ=17.6–18.8 ps at 400 K. For N_2 the low-loading residence times are τ=18–25 ps at 200 K and τ=10–13 ps at 300 K. These results clearly show the dependence on the relative quadrupole moments of CO_2 and N_2. The residence times for both CO_2 and N_2 monotonically increase with loading. As molecules attempt to leave, other molecules nearby block them from entering other basins. A linear relationship of $(1+\theta)$ correlates the residence times remarkably well for this case, where θ is the fractional loading based on eight channel sites per unit cell. However, this fit is not based on any physical argument. The residence times for the sinusoidal channel basins are larger by a small percentage compared to the values for the straight channels, since the sinusoidal channels are tortuous pathways, making it somewhat harder for the molecules to leave the channel basins.

The Arrhenius analysis for the residence times is presented in Fig. 7a for the case of 2 CO_2 molecules per unit cell at 200, 300, and 400 K. Fig. 7b compares the activation energy barriers for silicalite-1, calculated from the residence time analysis and from the self-diffusivity. Even though the temperature range is narrow, agreement is fairly good. The two sets of activation barriers agree within a fraction of a R_gT (e.g. R_gT=1.67 kJ/mole at 200 K). The discrepancy between the two types of calculations is due to the weak activation barriers for CO_2 and N_2 diffusion in silicalite-1, where molecules can easily jump into neighboring basins, reside for a short period, and then depart again for other basins. Attempts to cross an activation barrier may also be unsuccessful, so that a molecule returns to its origin after attempting to cross. These short time contributions create overall lower displacements when calculating the diffusivities, but appear in the residence time measurements as shorter time samples.

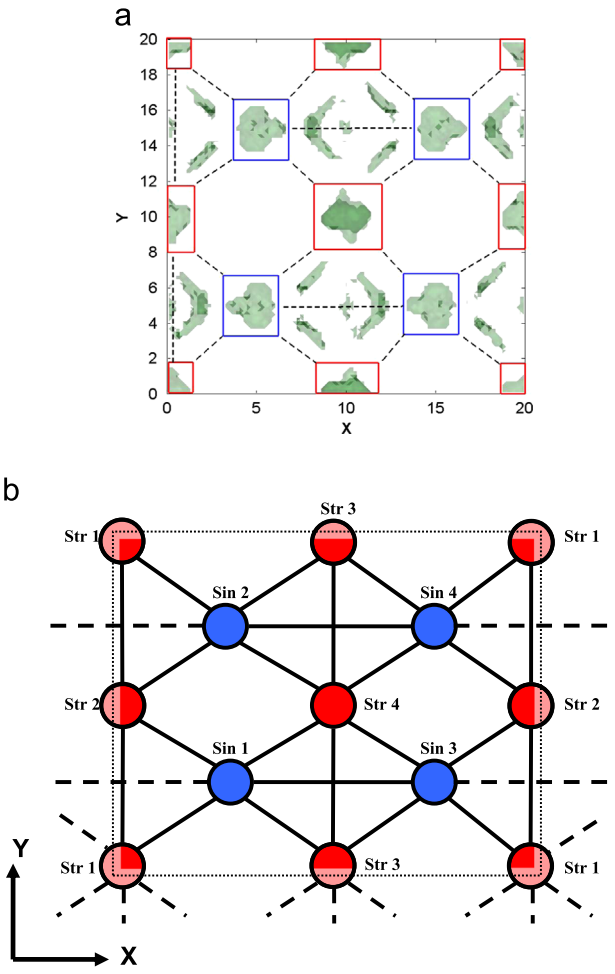

Fig. 5. (a) The stable basins identified from the MD simulation of 4 CO_2/Unit Cell of silicalite-1 at 200 K, using threshold density 0.01 $Å^{-3}$. Coordinates are in Å. The red boxes and nodes indicate the straight channel basins, while the blue boxes and nodes indicate the sinusoidal channel basins. (b) A coarse-grained representation of the ZSM-5 lattice, in which the nodes are stable basins and the bonds are effective jumps (over the intersections). A similar lattice representation is used for ZSM-5 with Si/Al=95 (see Newsome et al., 2014). (For interpretation of the references to color in this figure legend, the reader is referred to the web version of this article.)

3.6. Residence times for CO_2 and N_2 in Na-ZSM-5 with Si/Al=95

ZSM-5 with Al and Na^+ cations is next considered, to determine the role energetic heterogeneity plays on the residence times. The residence times of CO_2 in the eight channel basins are presented in Fig. 8a and b at 200 K, in Fig. 8c and d at 300 K, and in Fig. 8e and f at 400 K. For this particular case, the basins are classified as strong, moderate, and weak in energetic strength, since the cations change the shape of the potential energy landscape.

There is one cation per unit cell. As this cation is placed at an intersection, molecules can access the cation from either a sinusoidal or straight channel, creating two strong basins, designated as Sin1 and Str1. The cation effectively separates these two strong basins, via partial pore blockage, as it becomes more difficult for molecules to bypass the cation. In silicalite-1 the intersections could be ignored as basins, but, when Si/Al=95, the intersection with the cation is considered to be part of one of the strong basins, Sin1. The three other intersections, without cations, were treated in the same way as for silicalite-1.

The basin Sin3 is spatially close to Sin1, preventing any distinct spacing between the basin volumes, as was done for silicalite-1 by

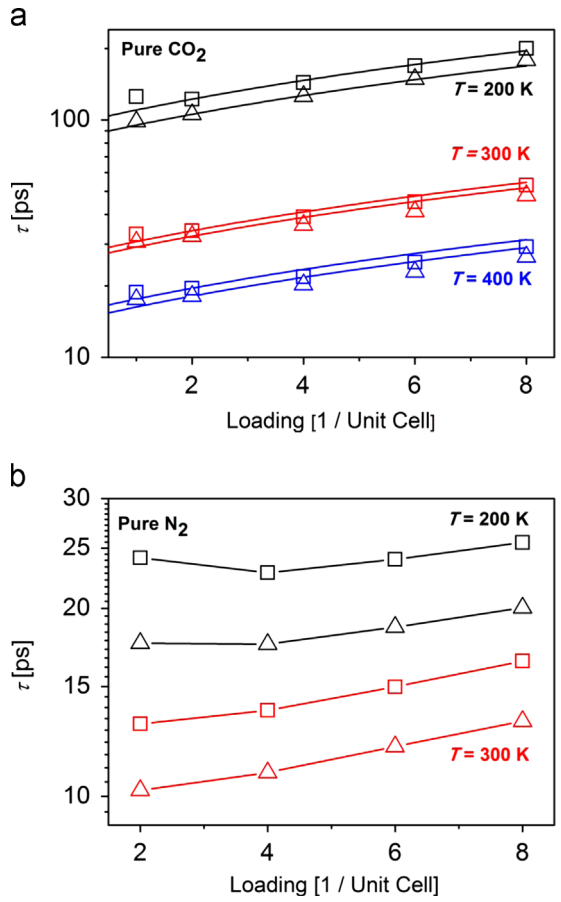

Fig. 6. Residence times of (a) pure CO_2 and (b) pure N_2 in silicalite-1 at 200, 300, and 400 K. The residence times are plotted on a $\log_{10}$ scale due to the wide range of values. The squares correspond to the sinusoidal channel and the triangles correspond to the straight channel. The black, red, and blue curves are for 200, 300, and 400 K, respectively. (For interpretation of the references to color in this figure legend, the reader is referred to the web version of this article.)

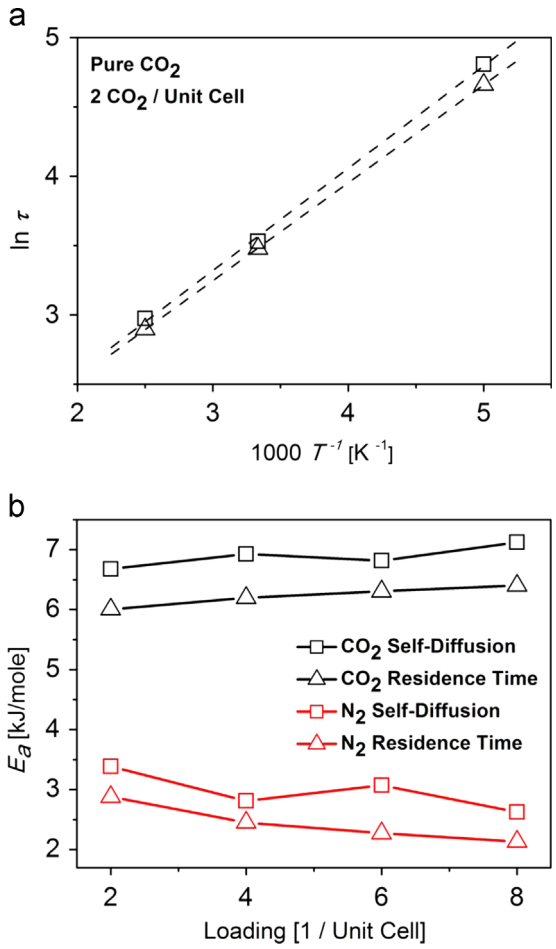

Fig. 7. (a) Arrhenius analysis of the residence times of CO_2 for the case of 2 CO_2/Unit Cell in silicalite-1 in the range of 200–400 K. (b) Summary of activation energy barriers of CO_2 and N_2 in silicalite-1, comparing residence times and self-diffusion results.

using the intersections as the separation zone. An analysis of the isosurface plots indicated that Sin3 is a distinct basin. Therefore, two options exist to handle this basin: it can be effectively included in the strong basin, or it can be considered as a separate basin, as done in silicalite-1. For this analysis the second option was chosen, as it is does not seem logical to remove basins merely because they are weaker in strength. Doing this would artificially increase the residence times associated to Sin1, as molecules would leave this basin less often.

The effect of the cation is most impressive at 200 K for CO_2, where the relative strength of the activation barrier near the cation is highest, as seen in Fig. 8a and b. The residence time of CO_2 at Sin1 is $\tau = 2 \times 10^3$ ps at low loading, then decreases with loading to $\tau = 540$ ps at 8 CO_2/Unit Cell. For Str1 the residence time also shows a dramatic decrease, where $\tau = 1.67 \times 10^3$ ps at low loading, then decreasing to $\tau = 800$ ps for 8 CO_2/Unit Cell. For comparison, the low-loading residence times in silicalite-1 are in the range $\tau = 98$–125 ps. At low loading CO_2 molecules spend more time near a cation. When a molecule hops to a weaker basin, it can easily return to the cation or hop to another one. At increased loading, molecules compete to adsorb on the cations, displacing each other and hindering access to the cations. This causes an increased chance for the molecules to hop to other, weak basins, so that the average residence times for the strong sites decrease with loading, at least at 200 K. The residence time for Str1 is less sensitive to loading compared to Sin1, as it is better surrounded by the zeolite lattice (as observed in density isosurface plots). Sin1 is more exposed, since it includes the volume of the nearby intersection, making it more accessible.

The Sin3 basin is labeled as of moderate strength, due to its intermediate value of $\tau = 330$–379 ps over all loadings. Str2 is also designated as a moderate basin, with $\tau = 390$–465 ps over all loadings. The residence times of Sin3 and Str2 are shorter than for Sin1 and Str1, but longer than residence times for basins Sin2, Sin4, Str3, and Str4, which are in the range of $\tau = 64$–300 ps, which can be designated as weak basins. The residence times for these weaker basins mostly increase with loading, since the CO_2 molecules spend more time at the weaker basins at higher loading as they become competitively displaced away from the cations and also must compete with other molecules at higher loading, due to a crowding effect. However, at relatively low loadings, a decrease in residence time, to a minimum around 3 molecules/unit cell, is noted for Sin4 and Str4.

Fig. 8c and d shows the residence times of CO_2 at 300 K, which are up to 370 ps on a strong site. For comparison, in silicalite-1 at 300 K $\tau = 33$–53 ps. At this higher temperature the residence times are substantially lower, but show qualitatively similar trends to the residence times at 200 K. The Sin1 residence times are $\tau = 370$ ps at low loading, decreasing to $\tau = 190$ ps for 8 CO_2/Unit Cell. For Str1 $\tau = 170$ ps at low loading, decreases to $\tau = 140$ ps, then increasing to $\tau = 160$ ps. These trends for residence times on strong sites are consistent with those for CO_2 diffusivities in the same system: the mild decrease in residence times correlates to a mild increase in diffusivities at low loading (see Fig. 2b). The residence times of CO_2

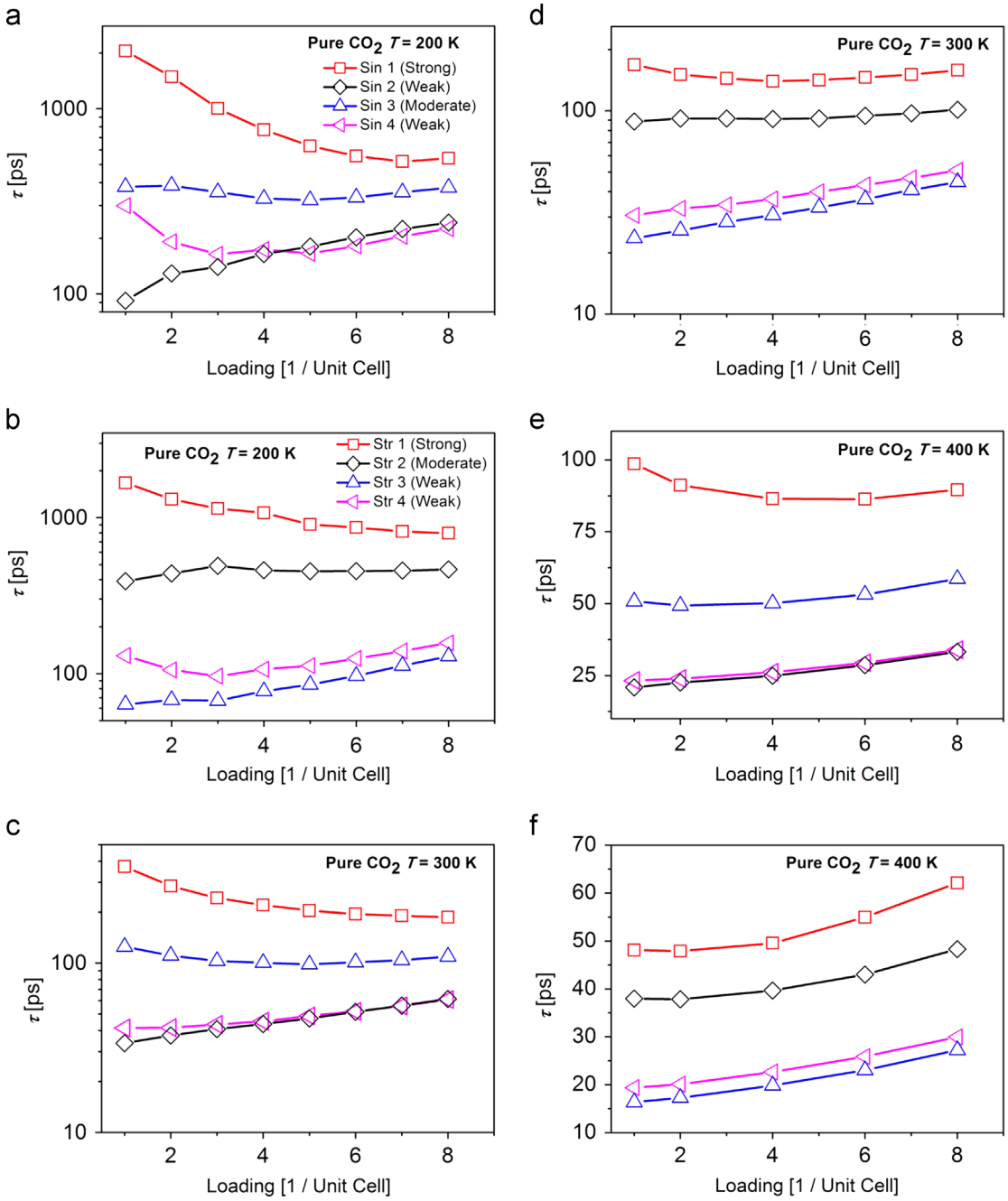

Fig. 8. Residence times of CO_2 in Na-ZSM-5 with Si/Al=95 over a range of temperature and loading, where the results are plotted for each specific channel, (a) the four sinusoidal channels at 200 K, (b) the four straight channels at 200 K, (c) the sinusoidal channels at 300 K, (d) the straight channels at 300 K, (e) the sinusoidal channels at 400 K, and (f) the straight channels at 400 K.

on the moderate basin Sin3 has a value of τ=105–125 ps at 300 K, relative to τ=330–380 ps at 200 K. For the other moderate basin Str2, τ=90 ps at low loading, then increasing to τ=100 ps with loading. The weak basins Sin2, Sin4, Str3, and Str4 have values in the range τ=24–61 ps, which increase with loading.

The residence times for CO_2 were also determined at 400 K, and presented in Fig. 8e and f. As expected, the residence times were much shorter for all the basins, and the cations had a diminished impact at this higher temperature as well. The residence time for Sin1 was τ=100 ps at low loading, decreasing to τ=90 ps around 8 CO_2/Unit Cell: for Str1 τ=48 ps at low loading, but now increased to τ=62 ps at higher loading. At 200 K the residence times for Str1 decreased with loading, while at 300 K they were effectively independent of loading. At this higher temperature the molecular competition becomes less relevant for both strong basins. For comparison, τ=18–30 ps in silicalite-1 at 400 K (see Fig. 6a). These nearly constant residence times are consistent with the trend for Na-ZSM-5 with Si/Al=95 at 400 K, as in Fig. 2c, where the self-diffusivities monotonically decrease. Sin3 is still labeled as a moderate basin, with a nearly constant τ=51–59 ps. For the so-called moderate basin Str2, τ=38 ps at low loading, increasing to τ=48 ps at higher loading. The weaker basins, Sin2, Sin4, Str3, and Str4, have residence times in the range τ=16–48 ps, which is essentially the range observed for silicalite-1. At this higher temperature, the distinction between strong, moderate, and weak basins is diminished.

The residence times for N_2 were also determined, so as to examine the effect of a smaller quadrupole moment on the residence

times. Fig. 9a and b shows the residence times for N_2 at 200 K. In the basin Sin1 $\tau=61$ ps at low loading, but mildly decreases to $\tau=56$ ps. For the second strong basin Str1, $\tau=35$–38 ps at all loadings. The competition effect observed for CO_2 in the strong basin at low temperature is clearly absent for N_2. The six other channel basins all fall within the same range of $\tau=17$–37 ps and increase with loading; the notion of moderate strength for Sin3 and Str2 is inapplicable even at this low temperature. The overall magnitude and qualitative dependence with respect to loading for N_2 at 200 K is similar as that for CO_2 at 400 K, where the effect of the cations was minimal.

The residence times for N_2 at 300 K are shown in Fig. 9c and d. The residence time for N_2 at Sin1 is $\tau=23$ ps at low loading, only slightly increasing to $\tau=28$ ps for 8 N_2/Unit Cell. In this example, the residence time of N_2 at Sin1 increases with loading, unlike the behavior for CO_2 or for N_2 at 200 K, where it decreases with loading. For Str1 $\tau=15$ ps at low loading, then increases to $\tau=20$ ps. In the other examples the residence times for this basin decreased with loading. Also in this example there is no meaningful difference between the two strong basins and the other weak basins, as the cations have no meaningful impact, where the quadrupole moment is low and the temperature is sufficiently high. The residence times for the other basins are in the range $\tau=11$–21 ps, and increase with loading.

An Arrhenius analysis was also performed for these residence times to extract the activation energy barriers. The molecules primarily spend their time in the stronger basins, especially for CO_2. Therefore, the average of the activation energy barriers for the two strongest basins is presented in Fig. 10 and compared to the activation energies calculated from the self-diffusivity. The agreement between these barriers is close, within 1 R_gT. The results for CO_2 virtually coincide with the notable exception of 2 CO_2/Unit Cell. From the Arrhenius analysis of the self-diffusivities, $E_a=12$ kJ/mole, while from the residence times $E_a=10$ kJ/mole. This is a distinct difference compared to the activation barriers at higher loadings, where the agreement systematically improves. The CO_2 molecules have a higher chance of returning to and staying in the strong basins relative to the other basins, reducing the net displacement. Hence, even though they are closely related, the activation energy barrier associated to the self-diffusivity must be higher than the activation energy barrier associated to the residence time. At higher loading the increased competition effect prevents this ease of return, so that the activation barriers become more consistent. The activation barriers are self-consistent for N_2 over all loadings, as the smaller quadrupole moment prevents any correlation with the cations. In fact, the motion of N_2 is hardly activated at all under these conditions ($E_a < 3R_gT$).

4. Conclusion

Diffusion of CO_2 and N_2 were studied by molecular dynamics simulations over a range of temperatures and loadings in silicalite-1 and in Na-ZSM-5, with Si/Al=95, and Si/Al=47. The extra-framework Na^+ cations substantially impact the diffusion of CO_2 and N_2. At the lower temperatures of 200 and 300 K, the diffusivities of CO_2 for Si/Al=95 initially increase with loading, before decreasing at higher loading. Only at 400 K does the self-diffusivity of CO_2 monotonically decrease for the three cation levels in this study, while the collective (or corrected) diffusivity is almost independent of loading. In contrast, the diffusivity of N_2

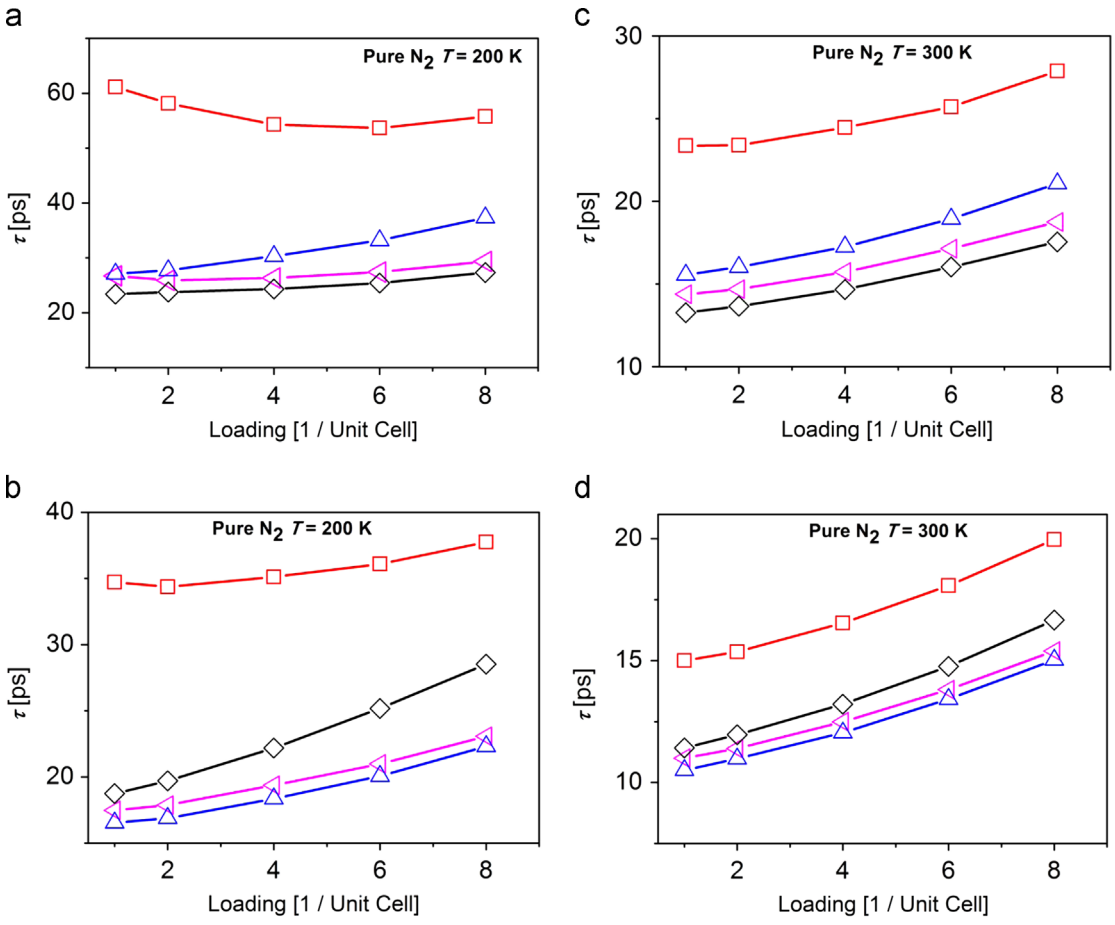

Fig. 9. Residence times of N_2 in Na-ZSM-5 with Si/Al=95 for sites in (a) the sinusoidal channels at 200 K, (b) the straight channels at 200 K, (c) the sinusoidal channels at 300 K, and (d) the straight channels at 300 K. See Fig. 8 for symbols legend.

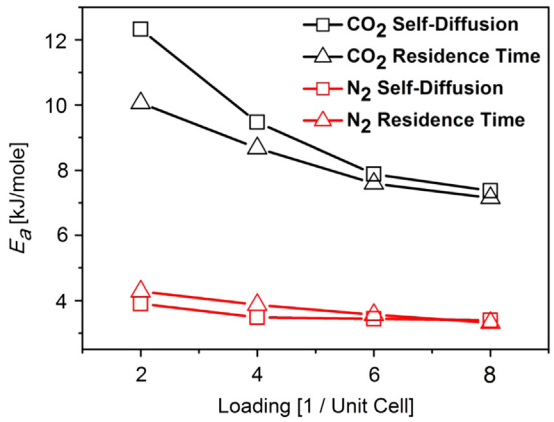

Fig. 10. Summary of activation energy barriers of CO_2 and N_2 in Na-ZSM-5 with Si/Al=95, taken from both the residence times and self-diffusivities. For the activation energy barriers derived from the residence times, the average of the two highest barriers is presented, since the molecules are predominately affected by these.

does not increase with loading in the low-loading regime for Si/Al=95 and 47. The magnitude of the self- and collective diffusivities decreases with lower Si/Al, but trends are similar to those for silicalite-1. Note that, again, the collective diffusivity is almost independent of loading.

The residence time for CO_2 near a Na^+ cation can increase by an order of magnitude or more when compared to silicalite-1, consistent with the substantial decrease in diffusivity. At 400 K the residence time for CO_2 near Na^+ sharply decreases, leading to higher values for the self-diffusivity, which still decreases with loading in a monotonic manner. The residence time of N_2 also increases near a cation, but variations between sites are not as large compared to CO_2.

These simulation results demonstrate the inherent complexity of analyzing the molecular mobility in the potential energy landscape of zeolite pore networks that include extra-framework Na^+ cations. A remarkable result is that the stable basins in silicalite-1 can be easily separated by only considering channels, at least for molecules such as CO_2 and N_2. Such ease of separation is not possible in Na-ZSM-5, so some degree of approximation was made, based on the near proximity of weak and strong basins, associated to Na^+. However, also in this case, a coarse-grained lattice representation with residence times associated to sites corresponding to different stable basins is possible. This is very useful as input to dynamic Monte Carlo simulations or mean field theory calculations, as part of a multi-scale approach to model diffusion in zeolites.

Some recommendations can be made for future studies. Extension of this study is possible to molecules of other polar light gases, such as CO, NO, H_2O, as well as O_2, in ZSM-5 with cations. A comprehensive data set could be compiled using the described methodology. This would be especially useful if coarse-grained lattice techniques are to be applied for systems with high energetic heterogeneity. The calculations could also be extended to different cation sizes, locations, and zeolite pore topologies, if different materials are to be considered as adsorbents or as active layers in membranes. Special care should be taken that the stable basins are properly defined, with inactivated but accessible regions excluded. In this particular case study, MD simulations showed that the intersections could be excluded as basins, but this will not always be the case. For example, for isobutane the intersections are the dominant basins and the channels are the separation zones (Vlugt et al., 2000).

One recommended strategy is to first develop the necessary MD algorithms and verify which, if any, conditions (temperature, loading, molecules, host environment, cation content) can be analyzed with stand-alone MD. It may be possible to use higher temperatures to first identify the location of the stable basins. Our proposed methodology is to use short-time MD simulations, which are accelerated using pre-tabulation methods, and to identify the different basins with associated residence times, which are parameters to coarse-grained simulations for longer time and length scales.

Nomenclature

D_S	self-diffusivity [m^2/s]
D_0	corrected or collective diffusivity [m^2/s]
E_a	activation energy barrier [kJ/mole]
t	time [ps]
r	position [Å]
h_a	Characteristic function [dimensionless]
R_g	universal gas constant [8.143 kJ/mole K]
T	temperature [K]
N_m	number of molecules [dimensionless]
N_t	number of time steps [dimensionless]
N_{events}	number of hopping events [dimensionless]
τ	residence time [ps]
θ	fractional loading [dimensionless]

Acknowledgments

The authors gratefully acknowledge funding from the European Union via STREP Project 014032 FUSION (Fundamental Studies of Transport in Inorganic Nanostructures). Part of the simulation work was carried out at computer clusters of the Technical University of Delft, Delft, the Netherlands and Rensselaer Polytechnic Institute, Troy, New York.

Appendix A. Supporting information

Supplementary data associated with this article can be found in the online version at http://dx.doi.org/10.1016/j.ces.2014.09.024.

References

Aoki, K., Tuan, V.A., Falconer, J.L., Noble, R.D., 2000. Gas permeation properties of ion-exchanged ZSM-5 zeolite membranes. Microporous Mesoporous Mater. 39, 485–492.
Auerbach, S.M., 2000. Theory and simulation of jump dynamics, diffusion and phase equilibrium in nanopores. Int. Rev. Phys. Chem. 19, 155–198.
Beerdsen, E., Dubbeldam, D., Smit, B., Vlugt, T.J.H., Calero, S., 2003. Simulating the effect of nonframework cations on the adsorption of alkanes in MFI-type zeolites. J. Phys. Chem. B 107, 12088–12096.
Beerdsen, E., Smit, B., Calero, S., 2002. The influence of non-framework sodium cations on the adsorption of alkanes in MFI- and MOR-type zeolites. J. Phys. Chem. B 106, 10659–10667.
Bernal, M.P., Coronas, J., Menendez, M., Santamaria, J., 2004. Separation of CO_2/N_2 mixtures using MFI-type zeolite membranes. AIChE J. 50, 127–135.
Bonelli, B., Civalleri, B., Fubini, B., Ugliengo, P., Areán, C.O., Garrone, E., 2000. Experimental and quantum chemical studies on the adsorption of carbon dioxide on alkali-metal-exchanged ZSM-5 zeolites. J. Phys. Chem. B 104, 10978–10988.
Bowen, T.C., Falconer, J.L., Noble, R.D., Skoulidas, A.I., Sholl, D., 2002. A comparison of atomistic simulations and experimental measurements of light gas permeation through zeolite membranes. Ind. Eng. Chem. Res. 41, 1641–1650.
Calleja, G., Pau, J., Calles, J.A., 1998. Pure and multicomponent adsorption equilibrium of carbon dioxide, ethylene, and propane on ZSM-5 zeolites with different Si/Al ratios. J. Chem. Eng. Data 43, 994–1003.
Chong, S.S., Jobic, H., Plazanet, M., Sholl, D., 2005. Concentration dependence of transport diffusion of ethane in silicalite: a comparison between neutron scattering experiments and atomically detailed simulations. Chem. Phys. Lett. 408, 157–161.
Choudhary, V.R., Nayak, V.S., Mamman, A.S., 1992. Diffusion of straight-chain and branched-chain liquid compounds in HZSM-5 zeolite. Ind. Eng. Chem. Res. 31, 624–628.

Coppens, M.-O., Bell, A.T., Chakraborty, A.K., 1999. Dynamic Monte Carlo and mean field study of the effect of strong adsorption sites on self-diffusion in zeolites. Chem. Eng. Sci. 54, 3455–3463.
Coppens, M.-O., Iyengar, V., 2005. Testing the consistency of the Maxwell–Stefan formulation when predicting self-diffusion in zeolites with strong adsorption sites. Nanotechnology 16, 442–448.
Daresbury Laboratory: DL_POLY MD Package. 2, 2003.
Dellago, C., Bolhuis, P.G., Geissler, P.L., 2001. Transition path sampling. Adv. Chem. Phys..
Demontis, P., Gulin-Gonzalez, J., Jobic, H., Masia, M., Sale, R., Suffritti, G.B., 2008. Dynamical properties of confined water nanoclusters: simulation study of hydrated zeolite NaA: structural and vibrational properties. ACS Nano 2, 1603–1614.
Demontis, P., Yashonath, S., Klein, M.L., 1989. Localization and mobility of benzene in sodium-Y zeolite by molecular dynamics calculations. J. Phys. Chem. 93, 5016–5019.
Dunne, J.A., Mariwals, R., Rao, R., Sircar, S., Gorte, R.J., Myers, A.L., 1996a. Calorimetric heats of adsorption and adsorption isotherms. 1. O_2, N_2, Ar, CO_2, CH_4, C_2H_6, and SF_6 on silicalite. Langmuir 12, 5888–5895.
Dunne, J.A., Rao, R., Sircar, S., Gorte, R.J., Myers, A.L., 1996b. Calorimetric heats of adsorption and adsorption isotherms. 2. O_2, N_2, Ar, CO_2, CH_4, C_2H_6, and SF_6 on NaX, HZSM-5, and NaZSM-5 zeolites. Langmuir 12, 5896–5904.
Frenkel, D., Smit, B., 2002. Understanding Molecular Simulation: From Algorithms to Applications, 2; .
Goj, A., Sholl, D., Akten, E.D., Kohen, D., 2002. Atomistic simulations of CO_2 and N_2 adsorption in silica zeolites: the impact of pore size and shape. J. Phys. Chem. B 106, 8367–8375.
Harlick, P.J.E., Tezel, F.H., 2002. Adsorption of carbon dioxide, methane, and nitrogen: pure and binary mixture adsorption by ZSM-5 with SiO_2/Al_2O_3 ratio of 30. Sep. Sci. Technol. 37, 33–60.
Harlick, P.J.E., Tezel, F.H., 2003. Adsorption of carbon dioxide, methane and nitrogen: pure and binary mixture adsorption for ZSM-5 with SiO_2/Al_2O_3 ratio of 280. Sep. Purif. Technol. 33, 199–210.
Harlick, P.J.E., Tezel, F.H., 2004. An experimental adsorbent screening study for CO_2 removal from N_2. Microporous Mesoporous Mater. 76, 71–79.
Hasegawa, Y., Tanaka, T., Watanabe, K., Jeong, B.H., Kusakabe, K., Morooka, S., 2002. Separation of CO_2–CH_4 and CO_2–N_2 systems using ion-exchanged FAU-type zeolite membranes with different Si/Al ratios. Korean J. Chem. Eng. 19, 309–313.
Hedin, N., DeMartin, G.J., Roth, W.J., Strohmaier, K.G., Reyes, S.C., 2008. PFG NMR self-diffusion of small hydrocarbons in high silica DDR, CHA and LTA structures. Microporous Mesoporous Mater. 109, 327–334.
Himeno, S., Tomita, T., Suzuki, K., Nakayama, K., Yajima, K., Yoshida, S., 2007. Synthesis and permeation properties of a DDR-type zeolite membrane for separation of CO_2/CH_4 gaseous mixtures. Ind. Eng. Chem. Res. 46, 6989–6997.
Hirotani, A., Mizukami, K., Miura, R., Takaba, H., Miya, T., Fahmi, A., Stirling, A., Kubo, M., Miyamoto, A., 1997. Grand canonical monte carlo simulation of the adsorption of CO_2 on silicalite and NaZSM-5. Appl. Surf. Sci. 120, 81–84.
Iyengar, V., Coppens, M.-O., 2004. Dynamic Monte-Carlo simulations of binary self-diffusion in zeolites: effect of strong adsorption sites. Chem. Eng. Sci. 59, 4747–4753.
Jee, S.E., Sholl, D., 2009. Carbon dioxide and methane transport in DDR zeolite: insights from molecular simulations into carbon dioxide separations in small pore zeolites. J. Am. Chem. Soc. 131, 7896–7904.
Jia, W., Murad, S., 2004. Molecular dynamics simulations of gas separations using faujasite-type zeolite membranes. J. Chem. Phys. 120, 4877–4885.
Jia, W., Murad, S., 2005. Separation of gas mixtures using a range of zeolite membranes: a molecular-dynamics study. J. Chem. Phys. 122, 234708.
Jobic, H., Skoulidas, A.I., Sholl, D., 2004. Determination of concentration dependent transport diffusivity of CF_4 in silicalite by neutron scattering experiments and molecular dynamics. J. Phys. Chem. B 108, 10613–10616.
Jobic, H., Theodorou, D., 2007. Quasi-elastic neutron scattering and molecular dynamics simulation as complementary techniques for studying diffusion in zeolites. Microporous Mesoporous Mater. 102, 21–50.
Jousse, F., Auerbach, S.M., 1997. Activated diffusion of benzene in Na-Y:rate constants from transition state theory with dynamical corrections. J. Chem. Phys. 107, 9629–9639.
June, R.L., Bell, A.T., Theodorou, D.N., 1991. Transition-state studies of xenon and SF_6 diffusion in silicalite. J. Phys. Chem. 95, 8866–8878.
Kärger, J., Pfeifer, H., 1991. Nuclear magnetic resonance measurement of mass transfer in molecular sieve crystallites. J. Chem. Soc., Faraday Trans. 87, 1989–1996.
Kärger, J., Pfeifer, H., Stallmach, F., Feoktistova, N.N., Zhdanov, S.P., 1993. ^{129}Xe and ^{13}C PFG nmr study of the intracrystalline self-diffusion of Xe, CO_2, and CO. Zeolites 13, 50–55.
Kärger, J., Ruthven, D., Theodorou, D.N., 2012. Diffusion in Nanoporous Materials. Wiley-VCH, Weinheim, Germany.
Katoh, M., Yamazaki, T., Ozawa, S., 1998. IR spectroscopic study of adsorption of binary gases over ion-exchanged ZSM-5 zeolites. J. Colloid Interface Sci. 203, 447–455.
Katoh, M., Yoshikawa, T., Tomonari, T., Katayama, K., Tomida, T., 2000. Adsorption characteristics of ion-exchanged ZSM-5 zeolites for CO_2/N_2 mixtures. J. Colloid Interface Sci. 226, 145–150.
Keil, F.J., Krishna, R., Coppens, M.-O., 2000. Modeling of diffusion in zeolites. Rev. Chem. Eng. 16, 71–197.
Koriabkina, A.O., de Jong, A.M., Hensen, E.J.M., van Santen, R.A., 2005. Concentration and temperature dependence of the diffusivity of n-hexane in MFI-zeolites. Microporous Mesoporous Mater. 77, 119–129.
Koriabkina, A.O., de Jong, A.M., Schuring, D., van Grondelle, J., van Santen, R.A., 2002. Influence of the acid sites on the intracrystalline diffusion of hexanes and their mixtures within MFI-zeolites. J. Phys. Chem. B 106, 9559–9566.
Liu, W., King, D., Liu, J., Johnson, B., Wang, Y., Yang, Z.G., 2009. Critical material and process issues for CO_2 separation from coal-powered plants. JOM 61, 36–44.
Makrodimitris, K., Papadopoulos, G.K., Theodorou, D., 2001. Prediction of permeation properties of CO_2 and N_2 through silicalite via molecular simulations. J. Phys. Chem. B 2001, 777–788.
Masuda, T., Fujikata, Y., Nishida, T., Hashimoto, K., 1998. The influence of acid sites on intracrystalline diffusivities within MFI-type zeolites. Microporous Mesoporous Mater. 23, 157–167.
Newsome, D., Gunawan, S., Baron, G., Denayer, J., Coppens, M.O., 2014. Adsorption of CO_2 and N_2 in Na–ZSM-5: effects of Na^+ and Al content studied by Grand Canonical Monte Carlo simulations and experiments. Adsorption 20, 157–171.
Papadopoulos, G.K., Jobic, H., Theodorou, D., 2004. Transport diffusivity of N_2 and CO_2 in silicalite: coherent quasielastic neutron scattering measurements and molecular dynamics simulations. J. Phys. Chem. B 108, 12748–12756.
Potoff, J.J., Siepmann, J.I., 2001. Vapor-liquid equilibria of mixtures containing alkanes, carbon dioxide, and nitrogen. AIChE J. 47, 1676–1682.
Ramanan, H., Auerbach, S.M., Tsapatsis, M., 2004. Beyond lattice models of activated transport in zeolites: high-temperature molecular dynamics of self-diffusion and cooperative diffusion of benzene in NaX. J. Phys. Chem. B 108, 17171–17178.
Saravanan, C., Auerbach, S.M., 1997a. Modeling the concentration dependence of diffusion in zeolites. 1. Analytical theory for benzene in NaY. J. Chem. Phys. 107, 8120–8131.
Saravanan, C., Auerbach, S.M., 1997b. Modeling the concentration dependence of diffusion in zeolites. 2. Kinetic Monte Carlo simulations of benzene in NaY. J. Chem. Phys. 107, 8132–8137.
Saravanan, C., Jousse, F., Auerbach, S.M., 1999. Kinetic theory and transition state simulation of dynamics in zeolites. Transition State Modeling for Catalysis, 721; , pp. 296–306.
Schuring, A., Auerbach, S.M., Fritzsche, S., 2007. A simple method for sampling partition function ratios. Chem. Phys. Lett. 450, 164–169.
Selassie, D., Davis, D., Dahlin, J., Feise, E., Haman, G., Sholl, D., Kohen, D., 2008. Atomistic simulations of CO_2 and N_2 diffusion in silica zeolites: the impact of pore size and shape. J. Phys. Chem. C 112, 16521–16531.
Siriwardane, R.V., Shen, M.S., Fisher, E.P., Poston, J.A., 2001. Adsorption of CO_2 on molecular sieves and activated carbon. Energy Fuels 15, 279–284.
Skoulidas, A.I., Sholl, D., 2003. Molecular dynamics simulations of self-diffusivities, corrected diffusivities, and transport diffusivities of light gases in four silica zeolites to assess influences of pore shape and connectivity. J. Phys. Chem. A 107, 10132–10141.
Skoulidas, A.I., Sholl, D.S., 2002. Transport diffusivities of CH_4, CF_4, He, Ne, Ar, Xe, and SF_6 in silicalite from atomistic simulations. J. Phys. Chem. B 106, 5058–5067.
Skoulidas, A.I., Sholl, D.S., Krishna, R., 2003. Correlation effects in diffusion of CH_4/CF_4 mixtures in MFI zeolite. A study linking MD simulations with the Maxwell–Stefan formulation. Langmuir 19, 7977–7988.
Smit, B., Maesen, T.L.M., 2008. Molecular simulations of zeolites: adsorption, diffusion, and shape selectivity. Chem. Rev. 108, 4125–4184.
Theodorou, D., Snurr, R.Q., Bell, A.T., 1996. Molecular dynamics and diffusion in microporous materials. . Comprehensive Supramolecular Chemistry, 7; , pp. 507–548.
van Koningsveld, H., van Bekkum, H., Jansen, J.C., 1987. On the location and disorder of the tetrapropylammonium (TPA) ion in zeolite ZSM-5 with improved framework accuracy. Acta Crystallogr. B43127.
Vlugt, T.J.H., Dellago, C., Smit, B., 2000. Diffusion of isobutane in silicalite studied by transition path sampling. J. Chem. Phys. 113, 8791–8799.
Voter, A., 1985. A Monte Carlo method for determining free-energy differences and transition state theory rate constants. J. Chem. Phys. 82, 1890–1899.
Walton, K.S., Abney, M.B., LeVan, D., 2006. CO_2 adsorption in Y and X zeolites modified by alkali metal cation exchange. Microporous Mesoporous Mater. 91, 78–84.
Wirawan, S.K., Creaser, D., 2006a. CO_2 adsorption on silicalite-1 and cation exchanged ZSM-5 zeolites using a step change method. Microporous Mesoporous Mater. 91, 196–205.
Wirawan, S.K., Creaser, D., 2006b. Multicomponent $H_2/CO/CO_2$ adsorption on BaZSM-5 zeolite. Sep. Purif. Technol. 52, 224–231.
Zhu, W.D., Hrabanek, P., Gora, L., Kapteijn, F., Moulijn, J.A., 2006. Role of adsorption in the permeation of CH_4 and CO_2 through a silicalite-1 membrane. Ind. Eng. Chem. Res. 45, 767–776.